New Insights on Choroidal Vascularity: A Comprehensive Topographic Approach

Abhilash Goud,[1] Sumit Randhir Singh,[1,2] Niroj Kumar Sahoo,[1] Mohammed Abdul Rasheed,[1] Kiran Kumar Vupparaboina,[1] Samatha Ankireddy,[3] Marco Lupidi,[4–6] and Jay Chhablani[1]

[1]LV Prasad Eye Institute, Hyderabad, India
[2]Retina and Uveitis Department, GMR Varalakshmi Campus, LV Prasad Eye Institute, Visakhapatnam, India
[3]University of Missouri, Kansas City School of Medicine, Kansas City, Missouri, United States
[4]Fondazione per la Macula Onlus, Di.N.O.G.Mi, University Eye Clinic, Università di Genova, Genova, Italy
[5]Department of Biomedical and Surgical Sciences, Section of Ophthalmology, University of Perugia, S. Maria della Misericordia Hospital, Perugia, Italy
[6]Centre de l'Odéon, Paris, France

Correspondence: Jay Chhablani, Smt. Kanuri Santhamma Centre for Vitreo-Retinal Diseases, LV Prasad Eye Institute, Banjara Hills, Hyderabad TG 500034, India; jay.chhablani@gmail.com.

AG and SRS are joint first authors.

Submitted: December 6, 2018
Accepted: July 7, 2019

Citation: Goud A, Singh SR, Sahoo NK, et al. New insights on choroidal vascularity: a comprehensive topographic approach. *Invest Ophthalmol Vis Sci*. 2019;60:3563–3569. https://doi.org/10.1167/iovs.18-26381

Purpose. To obtain a choroidal vascularity index (CVI) map of macular area on an Early Treatment Diabetic Retinopathy Study (ETDRS) grid.

Methods. The study was a cross-sectional study involving 30 eyes of 30 healthy individuals. In brief, a shadow-compensated automated algorithm was used to segment and binarize the individual optical coherence tomography (OCT) B-scans. This was followed by three-dimensional reconstruction of these processed B-scans to obtain the overall thickness and vascularity maps. ETDRS grid was overlaid on both the extrapolated thickness and vascularity maps to obtain the corresponding sector-wise CVI. The main outcome measure was to evaluate the topographical variation of CVI in the macular area.

Results. The mean age of the study participants was 44.33 ± 16.29 years (range, 18–70 years). CVI showed no significant difference in different rings, subfields, or quadrants of the ETDRS map. CVI had a negative correlation with age ($r = -0.384$, $P = 0.03$). There were no statistically significant differences between CVI of both eyes in either rings or the full ETDRS grid ($P = 0.30$) among normal subjects.

Conclusions. The variation in CVI does not follow similar patterns as seen in choroidal thickness (CT) in various locations. The novel choroidal vascularity mapping in the macular area may expand understanding on regional differences of choroidal vasculature in healthy eyes.

Keywords: optical coherence tomography, choroidal vascularity index, choroidal thickness

The choroid is the vascular coat of the eye and plays an important role in the physiology of the eye and the pathogenesis of various ocular diseases.[1,2] Choroidal thickness (CT) is a parameter that varies substantially both in healthy and in pathological conditions. It has been shown that subfoveal CT (SFCT) was higher in certain diseases such as central serous chorioretinopathy (CSCR), polypoidal choroidal vasculopathy (PCV), and uveitic conditions such as Vogt–Koyanagi–Harada (VKH) disease.[3,4] On the other hand, age-related macular degeneration (AMD) and pathological myopia (PM) were associated with a reduction in CT.[1,5,6] However, CT as an objective parameter is not a true representative of the entire choroidal vasculature and provides solely a bidimensional (2D) measurement at any specified point, limiting its utility.[2] The assessment of choroidal volume provides more robust anatomic details; however, fine details and quantitative data about the choroidal vascularity are difficult to determine with choroidal volume (CV) maps.[2]

Recently, the choroidal vascularity index (CVI), defined as the ratio of luminal area to total choroidal area, has been used as one of the biomarkers to evaluate the vascular status of the choroid.[7] Previous reports have concerned the role of the CVI in various disease entities including CSCR, PCV, panuveitis, VKH, and diabetic retinopathy.[7–11] The aforementioned studies calculated CVI from a single horizontal B-scan passing through the fovea, thus limiting understanding of structural changes to a single region. Moreover, in several diseases, the choroidal vascular changes are distributed in and beyond the macular area, making it imperative to study CT and CVI at various points for a true representation. We have reported the variation of CVI based on the scanning area comparing a single line scan through the fovea, central macular area of diameter 1 and 6 mm in the Early Treatment Diabetic Retinopathy Study (ETDRS) grid in normal eyes. However, the topographical variation of CVI in the macular area was not studied.[12] CT mapping has shown the variations of CT in the macular area, and other reports have identified SFCT as a predictor of CVI.[7,13,14] Thus, the variation of CVI in the macular area needs to be studied in detail.

The noise due to retinal blood vessels can affect optical coherence tomography (OCT) B-scans, thereby limiting the signal quality.[15] Our recent technique of shadow compensation and contrast enhancement helps to improve the quality of OCT scans, thus providing more accurate measurements.[15,16] In the current study, we evaluated the CVI in selected quadrants,

which was possible across the macular area (ETDRS map) using a shadow-compensated algorithm. In particular, we aimed to report ETDRS grid-based CVI mapping in volumetric OCT scans of healthy subjects.

Methods

This was an observational, cross-sectional study conducted at the LV Prasad Eye Institute, Hyderabad, India. The study was approved by the institutional review board (IRB) of the Institute, and all the methods adhered to the tenets of the Declaration of Helsinki.

All the study subjects signed a written consent form before being enrolled in the study and underwent a comprehensive eye examination including best-corrected visual acuity (BCVA), slit-lamp examination, and dilated fundus examination. The eligibility criteria included BCVA $\geq$ 20/25, age higher than 18 years, no history of prior ocular surgery, and no known ocular or systemic pathology potentially able to affect the choroidal vasculature. Therefore, exclusion criteria included subjects with any systemic diseases such as diabetes or hypertension, or eyes with known ocular diseases such as diabetic retinopathy, glaucoma, and any other retinal or optic disk pathology, high myopia (more than –6.00 diopters [D]), hyperopia (more than +1.5 D), anisometropia, and poor-quality OCT scans (poorly visible outer choroidal border). CVI in different areas of both eyes were compared. However, only the right eye of study subjects was considered for detailed analysis of CVI in various rings, subfields or quadrants.

OCT Measurements

All subjects underwent enhanced depth imaging OCT (EDI-OCT) scans using Spectralis OCT (Heidelberg Engineering, Heidelberg, Germany) in both eyes. The Spectralis OCT device provides 40,000 A-scans per second with a depth-in-tissue resolution of 7 μm and a transverse resolution of 14 μm using a superluminescent diode with wavelength of 870 nm.[17] A total of 31 raster scans centered on the fovea were performed. The raster scans covered a view of 20 × 20° (6 × 6 mm). A single B-scan consisted of 1024 A-scans (high-resolution mode). The scans were averaged using an automated real-time feature set at 25 frames, and subsequently, image analysis was done.

The proposed methodology for ETDRS-based choroid thickness and CVI mapping is addressed below. In particular, it involved (1) shadow compensation, (2) choroid localization, (3) binarizing choroidal layers, (4), three-dimensional (3D) mapping, and (5) ETDRS grid-based quantification. Specifically, on individual B-scans of each volume scan, steps 1, 2, and 3 were sequentially performed. Then the processed B-scans were 3D reconstructed for estimating the overall thickness and vascularity maps. In the following sections, the proposed methodology is described in detail.

Shadow Compensation and Image Enhancement

In general, OCT B-scans are noisy and contain shadows of the retinal blood vessels that affect the analysis of the deeper retinal layers and choroid.[16] In view of this, to facilitate a better visualization of choroidal structures, we began by performing a shadow compensation and a contrast enhancement on each B-scan.[16] In particular, we adopted Girard's approach, which restores the strongly attenuated image and uses an intensity-expansion to further provide a contrast enhancement.[15] In brief, first compressed pixel intensities of OCT B-scans were transformed to raw intensities using

$$J_{raw}(i,j) = \left(\frac{J(i,j)}{255}\right)^4, \quad (1)$$

where $J(i,j)$ is the intensity of the compressed image, and $J_{raw}(i,j)$ is the intensity of the raw image obtained by the OCT machine, both at location (i,j). Subsequently, the intensity-expansion operator (exponentiation) was used to increase the dynamic range of pixel intensities, which is given by

$$J_{exp}(i,j) = \frac{J_{raw}(i,j)}{2\sum_{k=i}^{p} J_{raw}(k,j)}, \quad (2)$$

where J_{exp} is the shadow-compensated image. In OCT imaging, a tissue at less depth produces higher intensity, compared to a similar tissue at a depth. Accordingly, to improve the signal strength, contrast enhancement was performed using

$$J_{enh}(i,j) = \frac{(J_{raw}(i,j))^n}{2\sum_{k=i}^{p} (J_{raw}(i,j))^n}, \quad (3)$$

where J_{enh} denotes the enhanced image and n denotes the exponentiation factor. Here, $n = 2$ was considered empirically.

Choroid Localization

The localization of the choroid is crucial in estimating CT as well as vascularity maps. We automatically localized the choroidal layer by detecting the choroidal inner and outer boundaries based on our previously validated method with nearly 96% Dice coefficient with reference to manual markings.[18] In particular, choroid inner boundary (CIB) was detected using gradient-based edge detection while the choroidal outer boundary (COB) was detected based on structural similarity (SSIM) index and tensor voting.[18] Figure 1 depicts the algorithmically detected boundaries on a representative image. The boundaries thus detected facilitated the segmentation of the choroidal layer as well as the binarized choroidal layer for obtaining thickness and vascularity index measurements.

Binarized Choroidal Layer

The quantification of the choroidal luminal and stromal regions for CVI measurements was obtained on binarized choroidal layer images, where the dark and bright pixels indicated the luminal and stromal regions, respectively. Specifically, we employed a recently reported exponential enhancement–based binarization method.[15,19] In brief, each OCT B-scan was subjected to adaptive histogram equalization, exponential enhancement (using an empirical exponentiation factor of 4), nonlinear enhancement, and thresholding, respectively, to increase the image contrast of choroid vessel structures and the dynamic range of pixel intensities. This also ensured a uniform distribution of pixel intensities across each A-scan and finally helped to obtain the binarized image. Subsequently, using the previously detected choroidal boundaries, the binarized choroidal layer was obtained.[19]

Choroidal Thickness Quantification

For each B-scan, thickness (in pixel units) along each A-scan (column) was first obtained by taking the difference between pixel locations of the choroidal outer and inner boundaries. Subsequently, thickness in pixel units was converted into micrometers based on the B-scan's axial and transverse resolutions.

Investigative Ophthalmology & Visual Science

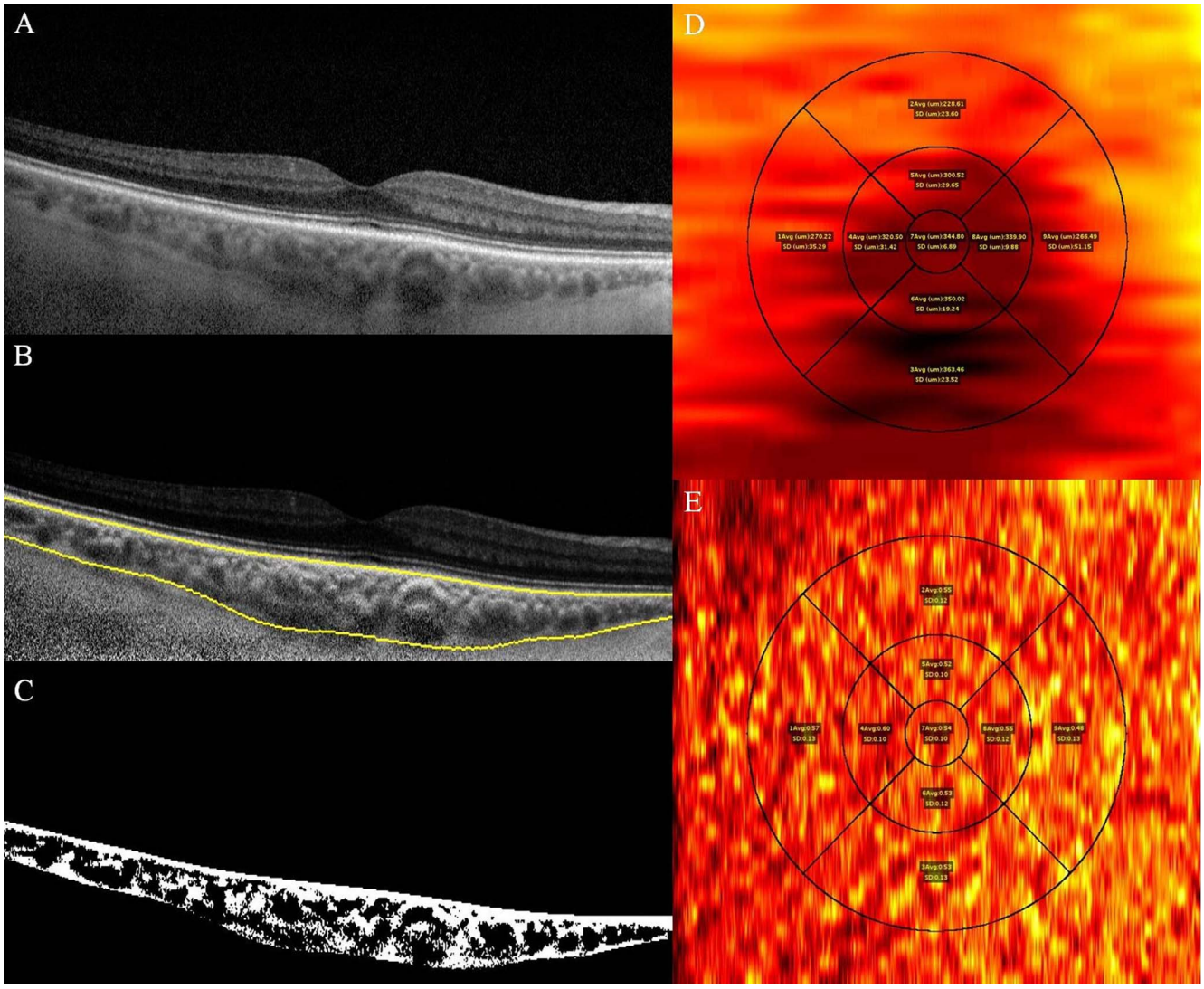

FIGURE 1. Enhanced depth imaging optical coherence tomography using Spectralis (Heidelberg Engineering) of the right eye of a 34-year-old female shows (**A**) OCT raw image, (**B**) choroid segmentation using an automated algorithm after shadow compensation, and (**C**) binarized image. (**D**) ETDRS grid-based choroidal thickness map shows mean and standard deviation of choroidal thickness at the center, the 3-mm zone, and the 6-mm zone in each quadrant. (**E**) ETDRS grid-based choroidal vascular index (CVI) map images shows mean and standard deviation of CVI at the center, the 3-mm zone, and the 6-mm zone in each quadrant. (**D**, **E**) *Red color* shows choroidal vessels and *yellow color* shows choroidal stroma.

Choroid Vascularity Index Quantification

As previously mentioned, the focus of the current study was in examining the choroidal vascularity index map, that is, understanding the variation of vascularity on a bidimensional en face view. In view of this, we estimated the vascularity index for each A-scan. In particular, we obtained the CVI index

$$CVI(i,j) = \frac{\begin{array}{c}Number\ of\ Pixels\ Belonging\ to\\ Luminal\ Region\ in\ an\ A-Scan\end{array}}{\begin{array}{c}Total\ Number\ of\ Pixels\\ Belonging\ to\ Choroid\ in\ an\ A-Scan\end{array}} \quad (4)$$

of each A-scan at location (i,j). Here i and j indicate the position of A-scan along lateral and transverse directions of the volume.

3D Mapping and ETDRS Grid-Based Quantification

As alluded to earlier, each volume scan covered an area of 6×6 mm. However, volume scan consists of only 31 B-scans taken with uniform separation. Consequently, there were missing data between the consecutive scans. In view of this, to obtain the complete volume data, bicubic interpolation was performed on estimated thickness and vascularity maps. Then, we overlaid the ETDRS grid on both the extrapolated thickness and vascularity maps to obtain the corresponding sector-wise statistics, specifically, mean and standard deviation (SD). In particular, while overlaying, centers for en face view of the volume scan and ETDRS grid were matched. ETDRS sectors were defined within the boundaries of three concentric rings. The innermost (foveal) ring centered at the fovea had a diameter of 1 mm. Inner and outer rings extended 1 to 3 and 3 to 6 mm from the fovea, respectively; thus, the total diameter of the outermost ring was 6 mm. For extracting sector-wise thickness and vascularity statistics, we obtained the thickness and vascularity index values of each sector based on indices obtained using connected components on a binarized ETDRS grid image. The ETDRS grid apart from the above-mentioned three rings was also subdivided into nine ETDRS subfields (e.g., center, inner superior, outer inferior) and four quadrants for analysis.

Statistical analysis was performed using SPSS statistical software version 22 (SPSS, Inc., Chicago, IL, USA). All values

Table 1. Mean, Standard Deviation, and Median Values of CVI in Different Subfields, Rings, and Quadrants

	Mean	Standard Deviation	Median
Subfields			
Center	0.465	0.082	0.473
Inner superior	0.472	0.081	0.475
Inner nasal	0.472	0.086	0.476
Inner inferior	0.456	0.088	0.481
Inner temporal	0.459	0.094	0.466
Outer superior	0.470	0.086	0.479
Outer nasal	0.477	0.091	0.490
Outer inferior	0.467	0.078	0.471
Outer temporal	0.477	0.088	0.485
Rings			
Center	0.458	0.082	0.472
Inner	0.465	0.082	0.478
Outer	0.473	0.081	0.468
Quadrants			
Superior	0.471	0.081	0.471
Nasal	0.475	0.087	0.488
Inferior	0.462	0.079	0.466
Temporal	0.468	0.085	0.469
Full ETDRS grid	0.465	0.079	0.473

were reported as mean ± standard deviation (SD). The comparisons of CVI in different circles, subfields, and quadrants were done using analysis of variance (ANOVA). Pearson's correlation test, independent *t*-test, and multiple linear regression analysis were done to determine the correlation between CVI and age, axial length, or sex. A *P* value of <0.05 was taken as statistically significant.

Results

Thirty eyes from 30 healthy subjects (19 females) were included in the study. The mean age was 44.3 ± 16.3 years, ranging from 18 to 70 years. Mean axial length was 23.53 ± 0.96 mm (range, 21.05–24.86 mm) with mean refraction (spherical equivalent) of –0.4 ± 1.2 D (range, –2.25 to +1.25 D). The mean CV of study subjects in the ETDRS grid was 18.65 ± 4.96 mm^3. The total stromal volume and vascular luminal volume were 9.15 ± 1.89 and 9.28 ± 3.45 mm^3, respectively. CVI in the innermost (foveal) ring was 0.46 ± 0.08. The corresponding CVI values in inner and outer ETDRS rings were 0.46 ± 0.08 and 0.47 ± 0.08, respectively ($P = 0.78$). The CVI values in the subfields and quadrants of ETDRS grid are shown in Table 1. There was no statistically significant difference in comparison of CVI in different subfields ($P = 0.99$) or quadrants ($P = 0.94$). Overall mean (±SD) CVI in the ETDRS grid was 0.46 ± 0.08.

Table 2 shows the correlations of CVI in the innermost (foveal) ring, inner and outer rings adjusted for age, axial length, or sex. CVI showed a negative correlation with age in the foveal ring ($P = 0.01$) while the inner ($P = 0.06$) and outer ring ($P = 0.08$) did not show a significant correlation. Overall, in the ETDRS grid, CVI had a negative correlation with age ($r = –0.384$, $P = 0.03$). The statistical significance was still present after adjusting for axial length ($P = 0.04$). The correlation of CVI with axial length in all circles did not yield statistically significant results, even after adjusting for age (Table 2). Similarly, CVI was not found to significantly differ for sex in foveal ($P = 0.73$), inner ($P = 0.96$), and outer rings ($P = 0.965$).

We assessed the potential correlation between CVI and different parameters by distinguishing ETDRS subfields and quadrants. The correlation of CVI and age was statistically significant in inner-inferior ($P = 0.03$), outer-superior, ($P = 0.03$), and outer-temporal ($P = 0.04$) subfields. The correlation of CVI with axial length and sex in any of the subfield was not significant (Supplementary Table S1). The quadrant-wise analysis of CVI correlation with age showed significant results in the temporal quadrant ($P = 0.04$) only, while axial length and sex correlation did not yield any statistically significant results (Supplementary Table S2).

Multiple regression analysis was done for variation of CVI with age, axial length, and sex in various rings (Table 3), subfields (Supplementary Table S3), and quadrants (Supplementary Table S4). CVI had a significant variation with age in the foveal ring ($P = 0.01$), the full ETDRS grid ($P = 0.04$) (Table 3), and inner-inferior ($P = 0.04$) and outer-superior subfields (*P*

Table 2. Correlation Between Average CVI at the Innermost (Foveal) Ring, Inner and Outer Ring With Age, Axial Length and Sex. The Correlation Between CVI and Age Was Statistically Significant at the Fovea ($P = 0.011$) and for the Full ETDRS Grid ($P = 0.036$)

	Pearson's Correlation Coefficient	*P*	Partial Correlation Coefficient	*P*
Innermost (foveal) ring				
Age, y	−0.458	**0.011**	−0.457	**0.013**, adjusted for AXL
Axial length, mm	−0.030	0.876	0.002	0.993, adjusted for age
Sex	n/a	0.705*	0.067	0.730, adjusted for AXL
Inner ring				
Age, y	−0.340	0.066	−0.337	0.074, adjusted for AXL
Axial length, mm	−0.064	0.738	−0.43	0.824, adjusted for age
Sex	n/a	0.900*	0.009	0.963, adjusted for AXL
Outer ring				
Age, y	−0.322	0.083	−0.318	0.093, adjusted for AXL
Axial length, mm	−0.076	0.689	−0.058	0.767, adjusted for age
Sex	n/a	0.890*	0.009	0.965, adjusted for AXL
Full ETDRS grid				
Age, y	−0.384	**0.036**	−0.382	**0.041**, adjusted for AXL
Axial length, mm	−0.058	0.761	−0.035	0.858, adjusted for age
Sex	n/a	0.825*	0.029	0.880, adjusted for AXL

The values were significant even after adjusting for axial length (*P* value of 0.013 and 0.041, respectively). Statistically significant *P* values are shown in bold. AXL, axial length; n/a, not applicable.

* Independent *t*-test.

Table 3. Multiple Linear Regression Analysis Results for CVI in the Various ETDRS Rings by Either Age, Axial Length, or Sex. A Statistically Significant Relationship Was Seen for Age at Center ($P = 0.015$) and for the Full ETDRS Grid ($P = 0.045$)

Factor	Coefficient	Standard Error	R^2	*P*
Center				
Intercept	0.516	0.379	0.213	0.185
Age	−0.002	0.001	0.213	**0.015**
Axial length	0.001	0.015	0.213	0.936
Sex	0.009	0.030*	0.213	0.760
Inner circle				
Intercept	0.622	0.397	0.117	0.129
Age	−0.002	0.001	0.117	0.079
Axial length	−0.003	0.016	0.117	0.831
Sex	0.000	0.032*	0.117	0.996
Outer circle				
Intercept	0.653	0.398	0.106	0.113
Age	−0.002	0.001	0.106	0.099
Axial length	−0.005	0.016	0.106	0.777
Sex	0.000	0.032*	0.106	0.997
Full ETDRS grid				
Intercept	0.597	0.380	0.149	0.128
Age	−0.002	0.001	0.149	**0.045**
Axial length	−0.002	0.015	0.149	0.883
Sex	0.003	0.030*	0.149	0.922

Statistically significant *P* values are shown in bold.
* Independent *t*-test.

= 0.04) (Supplementary Table S3). Figure 2 shows the scatter plot of CVI with age ($P < 0.04$) and axial length ($P < 0.88$).

We also compared the study eyes with fellow eyes of study subjects. Table 4 shows the mean, median, and standard deviations of ETDRS rings in both eyes. There were no statistically significant differences between the two eyes in either rings or the overall ETDRS grid.

Discussion

In this study, we proposed an ETDRS grid-based quantification of CVI mapping in volumetric OCT scans of healthy subjects using validated algorithms.[16,18,19] The results showed that overall vascular area is slightly lower than the stromal area (CVI = 0.46 ± 0.08). There was no significant difference in CVI in various rings, subfields, or quadrants in the ETDRS grid. CVI was found to have a statistically significant negative correlation with age ($P = 0.03$). Our study did not reveal any differences of

Table 4. Comparison of Mean of the Rings With the Fellow Eye (Independent *t*-Test)

	Right Eye			Left Eye			
Rings	Mean	SD	Median	Mean	SD	Median	*P* Value
Center	0.458	0.082	0.472	0.439	0.079	0.455	0.38
Inner	0.465	0.082	0.478	0.438	0.069	0.459	0.17
Outer	0.473	0.081	0.468	0.457	0.070	0.475	0.43
Full ETDRS grid	0.465	0.079	0.473	0.445	0.070	0.467	0.30

CVI between the study (right) and fellow (left) eye for any of the assessed parameters.

The pattern of the choroidal vasculature, especially the choriocapillaris, varies from the posterior pole to the retinal periphery. In vivo studies have reported that macular choroid has the maximum vascularity and the highest density of choriocapillaris.[20] However, in our study, we noted that central macular CVI was lower than other quadrants. This could be explained by the fact that although the SFCT is the highest,[21] the greater increase in stromal thickness more than overcompensates for the increase in vascular luminal areas in the macula, leading therefore to a reduction in the overall CVI. The increase in the stromal thickness of the choroid at the fovea is also explained by the presence of nonvascular smooth muscle cells in the outer choroid, which are particularly abundant in the macular area.[22]

In our study, the nasal subfields of the ETDRS grid had the higher CVI, which is in contrast to previously reported reduced CT and CV in nasal areas.[2,13] Consistent with the previous reports, CT and CV in nasal subfields (including inner nasal and outer nasal) was lower in our cohort as well.[2,13] However, the difference was not statistically significant. The discrepancy between the two parameters could be explained by the overall thinning of the choroid (especially the stromal component) in proximity to the disc and a possible disproportionate increase in the vascular component.

Previous studies have reported sex-wise differences in CT and CV, with males having a higher CT and CV, while a few other studies have not found any significant difference.[2,23–25] The intersex difference of CVI was not significant in our study. This suggests that although CV is higher in males, as reported in one of our previous publications,[2] CVI as a ratio may not be affected due to the proportionate reduction in both the luminal and stromal areas.

Our results showed no statistically significant difference in CVI between central to inner and outer circles. The possible

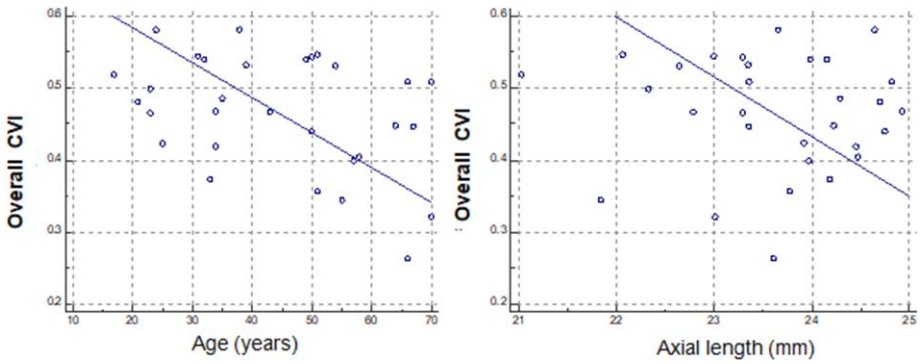

Figure 2. *Left*: scatter plot of overall choroidal vascularity index and age (years) in all subjects showing a statistically significant negative correlation ($P < 0.04$; $R^2 = 0.149$). *Right*: scatter plot of overall CVI and axial length (mm) showing a negative correlation, although not statistically significant ($P < 0.88$; $R^2 = 0.149$).

explanation could be the limited surface of the assessed area (within the vascular arcades). This ETDRS grid with a diameter of 6 mm may be insufficient to identify any significant variation of vascular caliber in normal individuals. Previous studies have evaluated CVI in normal subjects and disease conditions using macular and volumetric scans.[7–11] In conditions like CSCR, AMD, or PCV, where the pathology is localized in the form of either focal leak, polyps, or branching vascular network (BVN), changes in terms of CVI during the course of disease (natural history or after treatment) might provide substantial information about vascular changes. In such conditions, using ETDRS grid-based CVI calculation would be a helpful approach for clinicians to assess the disease progression and the treatment response.

Among the number of studies available on CVI, the main area of study has been subfoveal CVI or up to 750 μm on either side of the fovea using a single horizontal raster scan.[7,14] We have previously reported average CVI in the macular area. However, topographical variations of CVI in different circles or quadrants were not studied.[26] This study is unique since it evaluates CVI over the whole macular area to identify any significant physiological variation. CT has not been shown to vary significantly at either subfoveal or up to 2500 μm on either side of the fovea. CT has a negative correlation with age leading to a reduction of 1.18 μm/year.[27] The correlation between age and SFCT or CV has been previously reported ($r = -0.368$ and $r = -0.387$, respectively).[2] Considering CVI (luminal thickness) as an integral component in CT, reduction in CVI with age is expected. The correlation between age and CVI in our study sample ($r = -0.38$) was suggestive of a statistically significant negative correlation. Agrawal et al.[7] have reported a statistically significant direct correlation of CVI with SFCT ($P < 0.001$) while axial length ($P = 0.375$) was not significantly correlated. This finding highlights that CVI reduction with age parallels the changes in SFCT or CV. However, considering the fact that SFCT correlated well with CVI values and SFCT itself is dependent on axial length, the contribution of axial length to CVI cannot be underestimated. We excluded eyes with higher axial length and high refractive errors; thus, CVI values in our cohort cannot be extrapolated to high myopes or hypermetropes.

In this study, we employed fully automated and validated shadow compensation and binarization methods. Other attempts, for instance, those of Fabritius et al.[28] for shadow compensation and Kawano et al.[29] for binarization, were not fully automated and standardized. In particular, the method of Fabritius et al.[28] required to have an estimate (or localize) of segmented retinal vasculature of an en face image taken at the retinal pigment epithelium (RPE) plane. Indeed, almost all other attempts toward quantifying choroid vascularity have mostly adopted the Image J–based method of Sonoda et al.,[30] which is semiautomated, subjective, and tedious.[30] In contrast, our approach is fully automated and algorithmic performance was validated.[31,32] Although CVI values remain precise within studies, accuracy with respect to any specified gold standard such as histology needs to be established.[18,21,33] For instance, Wei et al.[34] have compared two commonly used binarization techniques; neither of these was found to be superior, and agreement between them was low. The inherent flaw with these algorithms exists because CVI calculation is based on the simple assumption that dark areas (vascular lumen) and light areas (stroma) are the only two constituents of the choroid. This kind of binary arrangement has not been conclusively proven in histologic studies.[1] The choroidal tissue at the posterior pole is known to have a segmental pattern and lobular arrangement composed of centrally located venule with curved arterioles.[20] However, these features are not identifiable on cross-sectional OCT scans. Moreover, differences in segmentation and thresholding techniques lead to differences in estimation of the choroidal area and/or luminal area. This explains the wide difference in CVI in various studies.[16,26,33,35,36]

Limitations of this study were the retrospective nature of the study and the small sample size. We had a limited number of patients in each age group with a narrow range of distribution of axial length and refraction. Moreover, the analysis of the distribution pattern of refraction revealed a skew toward myopia. Only the macular area was studied, which might not be representative of the vascularity of the entire fundus. Moreover, the study included healthy eyes, and the results cannot be extrapolated to various disease entities. OCT-based studies on thickness measurements have shown an effect of axial length on ocular magnification especially in the transverse dimension. We unfortunately did not consider the effect of ocular magnification in our analysis. The effect of motion, tilt, and illumination between B-scans was not considered while deriving the final 3D volumetric dataset.

In conclusion, our study reports a novel choroidal vascularity mapping of the macular area. The shadow-compensated images provided higher image quality due to the noise reduction. This approach could be useful to evaluate localized changes in choroidal vascularity, complementary to choroidal and retinal volumes, enhancing our understanding on the pathogenesis of various chorioretinal diseases.

Acknowledgments

Disclosure: **A. Goud**, None; **S.R. Singh**, None; **N.K. Sahoo**, None; **M.A. Rasheed**, None; **K.K. Vupparaboina**, None; **S. Ankireddy**, None; **M. Lupidi**, None; **J. Chhablani**, None

References

1. Nickla DL, Wallman J. The multifunctional choroid. *Prog Retin Eye Res*. 2010;29:144–168.
2. Barteselli G, Chhablani J, El-Emam S, et al. Choroidal volume variations with age, axial length, and sex in healthy subjects: a three-dimensional analysis. *Ophthalmology*. 2012;119:2572–2578.
3. Gallego-Pinazo R, Dolz-Marco R, Gómez-Ulla F, et al. Pachychoroid diseases of the macula. *Med Hypothesis Discov Innov Ophthalmol*. 2014;3:111.
4. Maruko I, Iida T, Sugano Y, et al. Subfoveal choroidal thickness after treatment of Vogt–Koyanagi–Harada disease. *Retina*. 2011;31:510–517.
5. Wang S, Wang Y, Gao X, et al. Choroidal thickness and high myopia: a cross-sectional study and meta-analysis. *BMC Ophthalmol*. 2015;15:70.
6. Jonas JB, Forster TM, Steinmetz P, et al. Choroidal thickness in age-related macular degeneration. *Retina*. 2014;34:1149–1155.
7. Agrawal R, Gupta P, Tan K-A, et al. Choroidal vascularity index as a measure of vascular status of the choroid: measurements in healthy eyes from a population-based study. *Sci Rep*. 2016;6:21090.
8. Agrawal R, Chhablani J, Tan K-A, et al. Choroidal vascularity index in central serous chorioretinopathy. *Retina*. 2016;36:1646–1651.
9. Agrawal R, Li LKH, Nakhate V, et al. Choroidal vascularity index in Vogt-Koyanagi-Harada disease: an EDI-OCT derived tool for monitoring disease progression. *Trans Vis Sci Tech*. 2016;5(4):7.
10. Agrawal R, Salman M, Tan K-A, et al. Choroidal vascularity index (CVI)-a novel optical coherence tomography parameter for monitoring patients with panuveitis? *PLoS One*. 2016;11:e0146344.

11. Wei X, Ting DSW, Ng WY, et al. Choroidal vascularity index: a novel optical coherence tomography based parameter in patients with exudative age-related macular degeneration. *Retina*. 2017;37:1120–1125.
12. Agrawal R, Wei X, Goud A, et al. Influence of scanning area on choroidal vascularity index measurement using optical coherence tomography. *Acta Ophthalmol*. 2017;95:e770–e775.
13. Hirata M, Tsujikawa A, Matsumoto A, et al. Macular choroidal thickness and volume in normal subjects measured by swept-source optical coherence tomography. *Invest Ophthalmol Vis Sci*. 2011;52:4971–4978.
14. Kim M, Ha MJ, Choi SY, et al. Choroidal vascularity index in type-2 diabetes analyzed by swept-source optical coherence tomography. *Sci Rep*. 2018;8:70.
15. Girard MJ, Strouthidis NG, Ethier CR, et al. Shadow removal and contrast enhancement in optical coherence tomography images of the human optic nerve head. *Invest Ophthalmol Vis Sci*. 2011;52:7738–7748.
16. Vupparaboina KK, Dansingani KK, Goud A, et al. Quantitative shadow compensated optical coherence tomography of choroidal vasculature. *Sci Rep*. 2018;8:6461.
17. Puzyeyeva O, Lam WC, Flanagan JG, et al. High-resolution optical coherence tomography retinal imaging: a case series illustrating potential and limitations. *J Ophthalmol*. 2011; 2011:764183.
18. Vupparaboina KK, Nizampatnam S, Chhablani J, et al. Automated estimation of choroidal thickness distribution and volume based on OCT images of posterior visual section. *Comput Med Imaging Graph*. 2015;46:315–327.
19. Vupparaboina KK, Richhariya A, Chhablani J, et al. Optical coherence tomography imaging: automated binarization of choroid for stromal-luminal analysis. Paper presented at the Signal and Information Processing (IConSIP) International Conference, Vishnupuri, Maharashtra, India, October 2016.
20. Hayreh SS. In vivo choroidal circulation and its watershed zones. *Eye (Lond)*. 1990;4(Pt 2):273–289.
21. Branchini LA, Adhi M, Regatieri CV, et al. Analysis of choroidal morphologic features and vasculature in healthy eyes using spectral-domain optical coherence tomography. *Ophthalmology*. 2013;120:1901–1908.
22. May CA. Non-vascular smooth muscle cells in the human choroid: distribution, development and further characterization. *J Anat*. 2005;207:381–390.
23. Li XQ, Larsen M, Munch IC. Subfoveal choroidal thickness in relation to sex and axial length in 93 Danish university students. *Invest Ophthalmol Vis Sci*. 2011;52:8438–8441.
24. Zeng J, Liu R, Zhang X, et al. Relationship between gender and posterior pole choroidal thickness in normal eyes [in Chinese]. *Zhonghua Yan Ke Za Zhi*. 2012;48:1093–1096.
25. Akhtar Z, Rishi P, Srikanth R, et al. Choroidal thickness in normal Indian subjects using swept source optical coherence tomography. *PLoS One*. 2018;13:e0197457.
26. Agrawal R, Wei X, Goud A, et al. Influence of scanning area on choroidal vascularity index measurement using optical coherence tomography. *Acta Ophthalmol*. 2017;95:e770–e775.
27. Chhablani J, Rao PS, Venkata A, et al. Choroidal thickness profile in healthy Indian subjects. *Ind J Ophthalmol*. 2014;62: 1060.
28. Fabritius T, Makita S, Hong Y, et al. Automated retinal shadow compensation of optical coherence tomography images. *J Biomed Opt*. 2009;14:010503.
29. Kawano H, Sonoda S, Yamashita T, et al. Relative changes in luminal and stromal areas of choroid determined by binarization of EDI-OCT images in eyes with Vogt-Koyanagi-Harada disease after treatment. *Graefes Arch Clin Exp Ophthalmol*. 2016;254:421–426.
30. Sonoda S, Sakamoto T, Yamashita T, et al. Choroidal structure in normal eyes and after photodynamic therapy determined by binarization of optical coherence tomographic images. *Invest Ophthalmol Vis Sci*. 2014;55:3893–3899.
31. Rasheed M, Sahoo N, Goud A, et al. Qualitative comparison of choroidal vascularity measurement algorithms. *Indian J Ophthalmol*. 2018;66:1785–1789.
32. Vupparaboina KK, Dansingani KK, Goud A, et al. Quantitative shadow compensated optical coherence tomography of choroidal vasculature. *Sci Rep*. 2018;8:6461.
33. Agrawal R, Gupta P, Tan KA, et al. Choroidal vascularity index as a measure of vascular status of the choroid: measurements in healthy eyes from a population-based study. *Sci Rep*. 2016; 6:21090.
34. Wei X, Sonoda S, Mishra C, et al. Comparison of choroidal vascularity markers on optical coherence tomography using two-image binarization techniques. *Invest Ophthalmol Vis Sci*. 2018;59:1206–1211.
35. Rasheed MA, Sahoo NK, Goud A, et al. Qualitative comparison of choroidal vascularity measurement algorithms. *Indian J Ophthalmol*. 2018;66:1785–1789.
36. Singh SR, Invernizzi A, Rasheed MA, et al. Wide-field choroidal vascularity in healthy eyes. *Am J Ophthalmol* 2018;193:100–105.

Investigative Ophthalmology & Visual Science